

Interferometric Full-Waveform Inversion of Time-Lapse Data

Mrinal Sinha*, King Abdullah University of Science and Technology, Thuwal

SUMMARY

One of the key challenges associated with time-lapse surveys is ensuring the repeatability between the baseline and monitor surveys. Non-repeatability between the surveys is caused by varying environmental conditions over the course of different surveys. To overcome this challenge, we propose the use of interferometric full waveform inversion (IFWI) for inverting the velocity model from data recorded by baseline and monitor surveys. A known reflector is used as the reference reflector for IFWI, and the data are naturally redatumed to this reference reflector using natural reflections as the redatuming operator. This natural redatuming mitigates the artifacts introduced by the repeatability errors that originate above the reference reflector.

INTRODUCTION

4D seismic has been used successfully for monitoring reservoirs (Calvert, 2005; Lumley, 1995). Pumping out oil or injection of fluids over the life-cycle of an oilfield results in fluid movement in the subsurface which changes the seismic impedance of the reservoir. The main aim of 4D surveys is to be able to track this fluid movement using seismic imaging methods. One of the problems with 4D surveys is that the environmental conditions change over time so that the experiment is insufficiently repeatable. The water-layer velocity during a marine experiment changes with time because of the time-varying environmental conditions such as temperature, salinity, ocean currents and depth. For deepwater reservoirs these variations are even more pronounced since the water-column is very thick. These deviations lead to uncertainty in the estimation of the water-layer velocity, which can lead to image distortion similar to that caused by static errors in land data. In addition tidal variations will introduce statics shifts into marine data. Some of the repeatability errors can be overcome by using improved acquisition systems such as ocean bottom cables (OBC) where the receiver cable is deployed on the sea-floor, but these surveys are still not completely immune to repeatability errors. Therefore, repeatable surveys are a challenge for monitoring of reservoirs.

Multiscale full waveform inversion (FWI) can be used to resolve both the low- and high-wavenumber characteristics of the inverted models (Boonyasiriwat et al., 2010; Fichtner et al., 2013). This makes FWI an ideal choice for inverting for time-lapse changes in the subsurface medium. Recently, many applications of 4D FWI to recover temporal model variations have appeared in the literature (Routh et al., 2012; Queisser and Singh, 2013; Raknes and Arntsen, 2014) even though it is sensitive to non-repeatability errors (Asnaashari et al., 2012). Maharramov et al. (2016) simultaneously inverted the baseline and monitor datasets, while also imposing a model-regularization constraint to counter non-repeatability problems.

Another means for mitigating the non-repeatability problem was proposed by Zhou et al. (2006), who introduced the concept of interferometric migration. In this method they shifted the data by the traveltimes of the picked reference reflections. The time-shift can also be automatically computed by cross-correlating the trace windowed around the reference reflection with the original trace. This procedure is carried out for all the traces to theoretically cancel out the phase associated with the common raypaths above the reference interface. It also approximately redatumed the data to the reference interface without needing to know the velocity model. One problem, however, is that the correlated traces can lead to artifacts in the migration image and the reference reflections must be carefully windowed. To overcome this problem, the interferometric least-squares migration (ILSM) method was proposed by (Sinha and Schuster (2016)) where the migration artifacts are significantly reduced by iterative least-squares migration. Tests on synthetic and field data validated the effectiveness of this procedure.

We now extend the ILSM method to waveform inversion of time-lapse data. For time-lapse data, the reference reflector is selected and the correlated data are migrated at each iteration. Unlike ILSM, the background velocity is updated at each iteration.

The paper is organized into four sections. The introduction is followed by the theory of interferometric full-waveform inversion (IFWI). Numerical results on synthetic data are presented in the next section, followed by conclusions.

THEORY

We now derive the equations for IFWI. The derivation is similar to that for ILSM, except the final equations show that the velocity model is updated at each iteration.

Define the predicted trace in the frequency domain to be $D(\mathbf{g}|\mathbf{s})$ for a source at \mathbf{s} and geophone at \mathbf{g} . Let $D(\mathbf{g}|\mathbf{s})_{ref}$ denote the trace that is windowed around a reference reflection event as illustrated in Figure 1. To estimate the crosscorrelogram $\Phi(\mathbf{g}|\mathbf{s})$, the windowed reference reflections in the predicted data are temporally crosscorrelated with the predicted data. In the frequency domain, crosscorrelation is equivalent to the conjugated product of spectra

$$\Phi(\mathbf{g}|\mathbf{s}) = D(\mathbf{g}|\mathbf{s})D^*(\mathbf{g}|\mathbf{s})_{ref}, \quad (1)$$

which removes the 2-way propagation time from the surface to the reflector for near-offset traces. For example, denote the 2-way propagation time to the reference interface as $\tau_{sx_{ref}} + \tau_{x_{ref}g}$ so that $D(\mathbf{g}|\mathbf{s})_{ref} = e^{i\omega(\tau_{sx_{ref}} + \tau_{x_{ref}g})}$. If the reflection data from a deeper interface are given as $D(\mathbf{g}|\mathbf{s}) = e^{i\omega(\tau_{sx_0} + \tau_{x_0g})}$, then $D(\mathbf{g}|\mathbf{s})D(\mathbf{g}|\mathbf{s})_{ref}^* = e^{i\omega(\tau_{sx_0} + \tau_{x_0g} - \tau_{sx_{ref}} - \tau_{x_{ref}g})}$, where we conveniently ignore geo-

IFWI

metrical spreading effects by assuming, for example, that geometrical spreading effects have been compensated for by data processing. Thus, the deep reflection data have been naturally

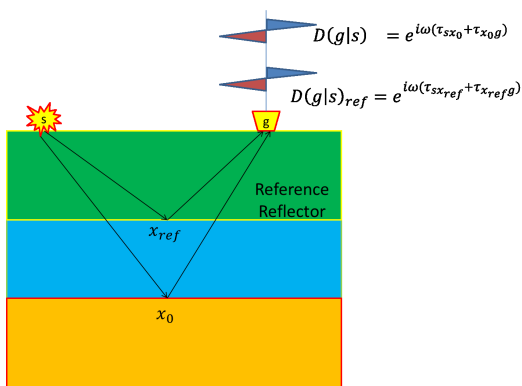


Figure 1: A crosscorrelogram is obtained by cross-correlating a recorded trace with the same trace windowed around the reference reflection.

redatumed to the reference reflector without knowing the velocity model. However, the implicit assumption is that the reflection rays for the reference reflection coincide with a portion of the rays associated with the deep reflection. Similarly, the observed crosscorrelogram $\tilde{\Phi}(\mathbf{g}|\mathbf{s})$ can be obtained by the crosscorrelation of recorded traces with the observed reference reflection traces.

The goal of IFWI is to find the velocity model which minimizes the squared L_2 norm of the difference between the observed and predicted crosscorrelograms,

$$\varepsilon = \frac{1}{2} \sum_{\omega} \sum_s \sum_g [\Phi(\mathbf{g}|\mathbf{s}) - \tilde{\Phi}(\mathbf{g}|\mathbf{s})]^2, \quad (2)$$

where we call this an interferometric waveform objective function. We will use an iterative gradient optimization method to achieve this goal, where the gradient of equation 2 with respect to the perturbation in slowness $s(\mathbf{x})$ is

$$\frac{\partial \varepsilon}{\partial s(\mathbf{x})} = \sum_{\omega} \sum_s \sum_g \frac{\partial \Phi(\mathbf{g}|\mathbf{s})}{\partial s(\mathbf{x})} [\Phi(\mathbf{g}|\mathbf{s}) - \tilde{\Phi}(\mathbf{g}|\mathbf{s})]. \quad (3)$$

Substituting the expression for predicted crosscorrelograms in equation 1 into equation 3 gives

$$\frac{\partial \varepsilon}{\partial s(\mathbf{x})} = \sum_{\omega} \sum_s \sum_g \overbrace{\frac{\partial D^*(\mathbf{g}|\mathbf{s})}{\partial s(\mathbf{x})}}^{\text{Migration kernel}} \overbrace{D(\mathbf{g}|\mathbf{s})_{\text{ref}} [\Phi(\mathbf{g}|\mathbf{s}) - \tilde{\Phi}(\mathbf{g}|\mathbf{s})]}^{\text{Interferometric residual}}, \quad (4)$$

where the Fréchet derivative $\frac{\partial D(\mathbf{g}|\mathbf{s})}{\partial s(\mathbf{x})}$ for the Helmholtz equation is given by Luo and Schuster (1991) as

$$\frac{\partial D(\mathbf{g}|\mathbf{s})}{\partial s(\mathbf{x})} = 2\omega^2 s(\mathbf{x}) G(\mathbf{g}|\mathbf{x}) G(\mathbf{x}|\mathbf{s}), \quad (5)$$

where $\mathbf{G}(\mathbf{x}|\mathbf{x}')$ is the Green's function for a receiver at \mathbf{x} and a point source at \mathbf{x}' , and $s(\mathbf{x})$ is the slowness value at the point

\mathbf{x} in the subsurface. The Fréchet derivative $\frac{\partial D(\mathbf{g}|\mathbf{s})_{\text{ref}}}{\partial s(\mathbf{x})}$ can be automatically set to zero by keeping the velocity model above the reference interface fixed. Equation 4 says that the interferometric gradient is formed by smearing the interferometric residual along the associated migration ellipses and wavepaths that resemble a pair of rabbit ears. In practice the convolution and crosscorrelation are implemented using time shifts.

Different Strategies for Time-Lapse Estimation

The standard way of estimating temporal changes in the slowness is by inverting the baseline and monitor datasets separately, and then the inverted monitor and baseline tomograms are subtracted from each other for estimating the temporal velocity variations in the reservoir. But the problem with this approach is that we might converge to two different local minima after inversion, and a subtraction of two such models will lead to spurious property changes.

Another approach is to use the velocity model inverted from the baseline data as an initial model for inverting the data from the monitor survey. Then the two models are subtracted from one another to evaluate the time-lapse velocity change. This assumes that the estimated baseline model is complete to the extent that when used as an initial model for inverting the monitor data all the extra updates are exclusively caused by reservoir changes. But in practice, we always get extra non-reservoir updates because the number of iterations used for inverting the baseline model is a finite number.

Yang et al. (2016) used double-difference waveform inversion (DDWI) to invert for time-lapse velocity changes and showed that DDWI provides a better estimate for the time-lapse changes compared to the previously discussed strategies. In this strategy the estimated baseline model is used as the initial model but instead of inverting the monitor data as a whole, we invert for the time-lapse difference between the baseline and monitor data sets. This is done by modifying the misfit as shown below

$$J(\mathbf{m}) = \sum_{\omega} \sum_s \sum_g \frac{1}{2} [(\mathbf{D}_{\text{mon}}(\mathbf{g}|\mathbf{s}) - \mathbf{D}_{\text{base}}(\mathbf{g}|\mathbf{s})) - (\mathbf{u}_{\text{mon}}(\mathbf{g}|\mathbf{s}, \mathbf{m}) - \mathbf{u}_{\text{base}}(\mathbf{g}|\mathbf{s}, \mathbf{m}_0))]^2. \quad (6)$$

Here, $\mathbf{D}_{\text{mon}}(\mathbf{g}|\mathbf{s})$ and $\mathbf{D}_{\text{base}}(\mathbf{g}|\mathbf{s})$ represent the observed monitor and baseline data for a source at \mathbf{s} and geophone at \mathbf{g} , respectively. $\mathbf{u}_{\text{mon}}(\mathbf{g}|\mathbf{s}, \mathbf{m})$ denotes the predicted data generated using model \mathbf{m} . $\mathbf{u}_{\text{base}}(\mathbf{g}|\mathbf{s}, \mathbf{m}_0)$ is the synthetic data generated using the baseline model \mathbf{m}_0 estimated by FWI and \mathbf{m} represents the velocity model for the monitor survey. Since the baseline model \mathbf{m}_0 has already been inverted for, \mathbf{u}_{base} remains fixed during DDWI. Similarly, by replacing the observed and predicted data by their respective crosscorrelogram components in equation 6, we obtain the misfit for double-difference interferometric full-waveform inversion (DDIFWI) as shown

below

$$J(\mathbf{m}) = \sum_{\omega} \sum_s \sum_g \frac{1}{2} [(\tilde{\Phi}_{mon}(\mathbf{g}|\mathbf{s}) - \tilde{\Phi}_{base}(\mathbf{g}|\mathbf{s})) - (\Phi_{mon}(\mathbf{g}|\mathbf{s}, \mathbf{m}) - \Phi_{base}(\mathbf{g}|\mathbf{s}, \mathbf{m}_0))]^2. \quad (7)$$

The gradient for this DDIFWI misfit is given by

$$\frac{\partial \epsilon}{\partial s(\mathbf{x})} = \sum_{\omega} \sum_s \sum_g \underbrace{\frac{\partial D_{mon}^*(\mathbf{g}|\mathbf{s})}{\partial s(\mathbf{x})}}_{\text{Migration kernel}} \underbrace{D(\mathbf{g}|\mathbf{s})_{ref}[(\tilde{\Phi}_{mon}(\mathbf{g}|\mathbf{s}) - \tilde{\Phi}_{base}(\mathbf{g}|\mathbf{s})) - (\Phi_{mon}(\mathbf{g}|\mathbf{s}, \mathbf{m}) - \Phi_{base}(\mathbf{g}|\mathbf{s}, \mathbf{m}_0))]}_{\text{Interferometric residual}} \quad (8)$$

NUMERICAL RESULTS

IFWI is tested on a 2-D model based on geology of the Gullfaks field in Norway (Raknes and Arntsen, 2014). A fixed-spread acquisition is used to generate the baseline data. The survey consists of 96 shots spaced at an interval of 60 m at a depth of 10 m below the sea surface. Each shot gather contains 301 receivers spread at an interval of 20 m. The velocity model used for generating baseline data and time-lapse changes in the velocity are shown in Figures 2a and 2b, respectively. To simulate non-repeatability in the monitor data, small variations on the order of 20 m/s to 40 m/s are introduced in the water layer, and the shot locations are randomly shifted to simulate tidal variations as shown in Figure 2b. The reservoir lies at the 2 km depth level as shown in Figure 2b. A 2-8 finite-difference scheme with a 6-Hz Ricker wavelet as the source signature is used to generate both the data sets. For the sake of simplicity, the baseline and monitor surveys are referred to as Year 1 and Year 2, respectively. Only reflections are inverted for both surveys. Figures 3a and 3b show the inverted models for Year 1 and Year 2 using FWI. Figure 4 shows the inverted IFWI tomo-grams for both the baseline and monitor surveys. Figures 5a and 5b show the time-lapse changes in velocity estimated by FWI and IFWI respectively, and the reservoir area is indicated by the black dashed box. The time-lapse change in the reservoir is recovered by both FWI and IFWI. However we also see spurious changes elsewhere because of the non-linearity of the inversion problem. IFWI provides a better estimate of the time-lapse changes compared to FWI.

Now we use DDFWI and DDIFWI to mitigate the spurious artifacts that are characteristic of the nonlinear inversion method. The tomograms inverted from the baseline surveys using FWI and IFWI are used as initial models for inverting the DDFWI and DDIFWI tomograms for Year 2. The tomograms inverted for Year 2 using DDFWI and DDIFWI are shown in Figure 6. The time-lapse change is computed by subtracting the monitor DDFWI and DDIFWI tomograms from their inverted baseline FWI and IFWI counterparts. Figure 7 shows the time-lapse change computed by DDFWI and DDIFWI. The time-lapse changes estimated by using double-difference waveform

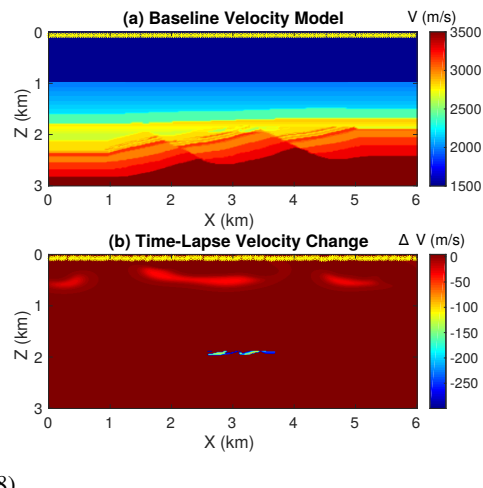


Figure 2: (a) Baseline velocity model and (b) time-lapse changes between the two surveys with shot locations indicated by yellow stars.

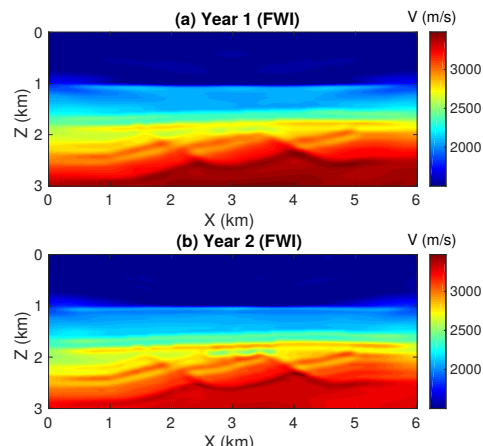


Figure 3: Inverted FWI (a) baseline and (b) monitor tomo-grams.

inversion is an improvement over the conventional method. DDIFWI highlights changes mostly at the reservoir level, whereas the DDFWI estimated time-lapse change indicate variations at not only the reservoir but also in non-reservoir areas where no actual changes occurred. These spurious changes are caused by non-repeatability errors added to the data. The double-difference approach combined with IFWI mitigates the spurious artifacts caused by overburden variations above the reference reflector, and provides an accurate estimate of the time-lapse changes in the reservoir area.

CONCLUSIONS

Synthetic results suggest that IFWI can overcome the challenge posed by time varying changes in the overburden and can provide an accurate velocity model below a specified ref-

IFWI

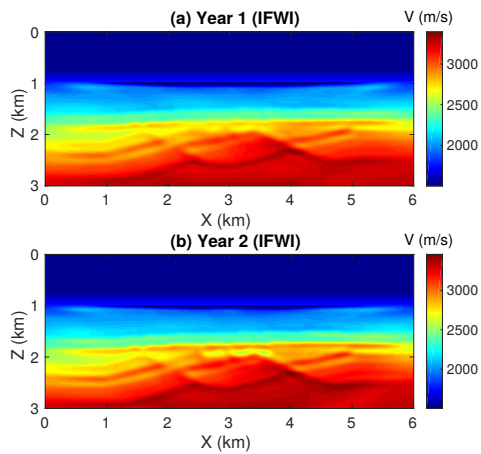


Figure 4: Inverted IFWI (a) baseline and (b) monitor tomograms.

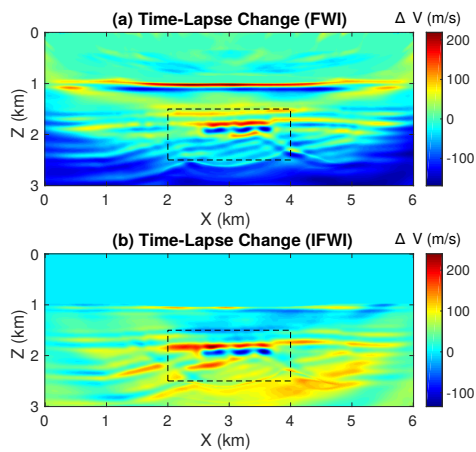


Figure 5: (a) Time-lapse tomograms computed by FWI and (b) IFWI.

erence reflector. Straightforward subtraction of baseline and monitor models can lead to false features in the estimated time-lapse change in the reservoir. The double-difference approach provides a more accurate estimate of the velocity variations in the reservoir by exclusively inverting for time-lapse changes in the waveform. A combination of double-difference and IFWI provides a much more reliable estimate of the property change inside the reservoir. The next step is to apply DDIFWI to time-lapse field data.

ACKNOWLEDGEMENTS

The research reported in this publication was supported by the King Abdullah University of Science and Technology (KAUST) in Thuwal, Saudi Arabia. We are grateful to the sponsors of the Center for Subsurface Imaging and Modeling (CSIM) Consortium for their financial support.

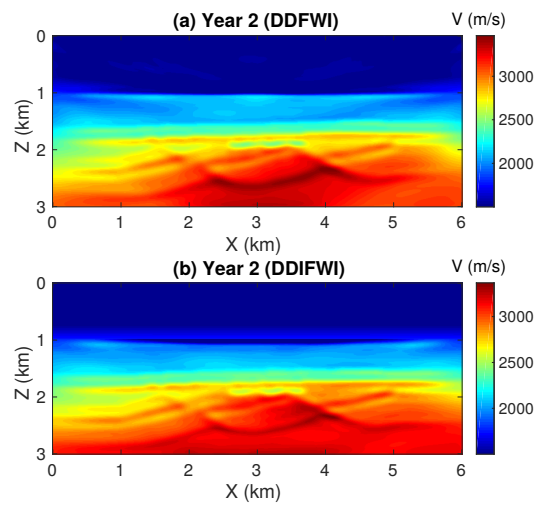


Figure 6: (a) Inverted monitor survey tomograms estimated using (a) DDFWI and (b) DDIFWI.

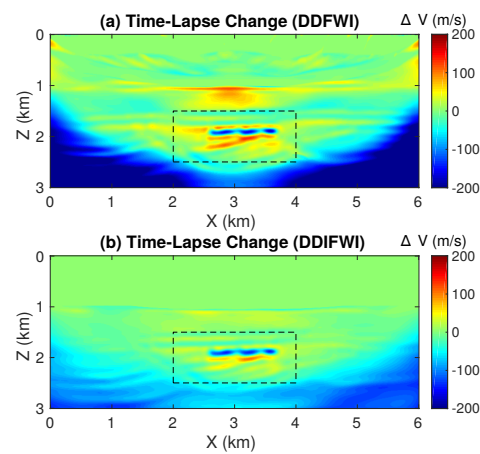


Figure 7: (a) Time-lapse tomograms computed by DDFWI and (b) DDIFWI.

EDITED REFERENCES

Note: This reference list is a copyedited version of the reference list submitted by the author. Reference lists for the 2017 SEG Technical Program Expanded Abstracts have been copyedited so that references provided with the online metadata for each paper will achieve a high degree of linking to cited sources that appear on the Web.

REFERENCES

Asnaashari, A., R. Brossier, S. Garambois, F. Audebert, P. Thore, and J. Virieux, 2012, Time-lapse imaging using regularized FWI: a robustness study: 82nd Annual International Meeting, SEG, Expanded Abstracts, 1–5, <https://doi.org/10.1190/segam2012-0699.1>.

Boonyasiriwat, C., G. T. Schuster, P. Valasek, and W. Cao, 2010, Applications of multiscale waveform inversion to marine data using a flooding technique and dynamic early-arrival windows: *Geophysics*, **75**, no. 6, R129–R136, <https://doi.org/10.1190/1.3507237>.

Calvert, R., 2005, Insights and methods for 4D reservoir monitoring and characterization: SEG/EAGE Distinguished Instructor Lecture Course, <https://doi.org/10.1190/1.9781560801696>.

Fichtner, A., J. Trampert, P. Cupillard, E. Saygin, T. Taymaz, Y. Capdeville, and A. Villase ~nor, 2013, Multiscale full waveform inversion: *Geophysical Journal International*, **194**, 534–556, <https://doi.org/10.1093/gji/ggt118>.

Lumley, D., 1995, Seismic time-lapse monitoring of subsurface fluid flow: PhD thesis, Stanford University.

Luo, Y., and G. Schuster, 1991, Wave equation travel time inversion: *Geophysics*, **56**, 645–653, <https://doi.org/10.1190/1.1443081>.

Maharramov, M., B. L. Biondi, and M. A. Meadows, 2016, Time-lapse inverse theory with applications: *Geophysics*, **81**, no. 6, R485–R501, <https://doi.org/10.1190/geo2016-0131.1>.

Queisser, M., and S. C. Singh, 2013, Full waveform inversion in the time lapse mode applied to CO₂ storage at Sleipner: *Geophysical Prospecting*, **61**, 537–555, <https://doi.org/10.1111/j.1365-2478.2012.01072.x>.

Raknes, E. B., and B. Arntsen, 2014, Time-lapse full-waveform inversion of limited-offset seismic data using a local migration regularization: *Geophysics*, **79**, no. 3, WA117–WA128, <https://doi.org/10.1190/geo2013-0369.1>.

Routh, P., G. Palacharla, I. Chikichev, and S. Lazaratos, 2012, Full wavefield inversion of time-lapse data for improved imaging and reservoir characterization: 82nd Annual International Meeting, SEG, Expanded Abstracts, 1–6, <https://doi.org/10.1190/segam2012-1043.1>.

Sinha, M., and G. Schuster, 2016, Mitigation of defocusing by statics and near-surface velocity errors by interferometric least-squares migration with a reference datum: *Geophysics*, **81**, S195–S206, <https://doi.org/10.1190/geo2015-0637.1>.

Yang, D., F. Liu, S. Morton, A. Malcolm, and M. Fehler, 2016, Time-lapse full-waveform inversion with ocean-bottom cable data: Application on Valhall field: *Geophysics*, **81**, R225–R235, <https://doi.org/10.1190/geo2015-0345.1>.

Zhou, M., Z. Jiang, J. Yu, and G. Schuster, 2006, Comparison between interferometric migration and reduced-time migration of common-depth-point data: *Geophysics*, **71**, S1189–S1196, <https://doi.org/10.1190/1.2213046>.